MODELING OF PRESSURE NON-UNIFORMITY AT A DIE SCALE FOR ILD CMP

Jihong Choi
Sponsored by NSF and FLCC

ABSTRACT

Local material removal rate is inversely proportional to the local pattern density in ILD CMP. With the assumption that the local velocity and Preston coefficient are constant across a die, local MRR non-uniformity is attributed to the local pressure non-uniformity. Pressure distributions on two different test patterns consist of five different pattern density sections were calculated with a finite element model. These pressure distributions were compared with semi-empirical pattern dependant oxide CMP model with three different weighting functions. Result showed that pressure distribution can be well approximated with the pattern density dependant oxide CMP model.

Keywords: ILD CMP, finite element modeling (FEM), pressure distribution, die scale.

INTRODUCTION

Die-scale non-uniformity in ILD CMP is mainly attributed to the non-uniformity of the pattern density across a chip. It was experimentally showed that local material removal rate in CMP is dominantly affected by the local pattern density (Ouma et al., 1997; Stirne et al., 1998).

The pattern density dependant oxide CMP model (Ouma et al., 2002) has been successfully used for a characterization of a CMP process and modeling of pattern dependant CMP performance in a die scale. Evaluating local pattern density is essential for the performance of a pattern density dependant oxide model. The concept of planarization length, which is determined by experiments, and weighting function is used for evaluating local effective pattern density. It has been showed that the elliptic weighting function from idealized pad deformation profile allows best result (Ouma et al., 2002). Even though this model has worked successfully, it is semi-empirical model, where the planarization length should be determined with test runs on test structures. For an integrated model of CMP process, which can be used for a process and consumable design optimization, a more analytical model that can be applied to general pattern should be developed. With the assumption that the local material removal rate follows Preston's model and local Preston coefficient and velocity is not much dependant on the local pattern density, local pressure becomes more dominantly dependant on the local pattern density.

$$MRR = K_e PV \qquad (1)$$

(Preston model (1927))

$$MRR = \frac{K}{\rho(x,y)} \tag{2}$$

(Pattern dependant oxide model (Ouma et al., 2002))

$$p(x,y) = \frac{K}{K_e V}\frac{1}{\rho(x,y)} = k\frac{1}{\rho(x,y)} \tag{3}$$

In this study, by using a finite element simulation, contact stress distributions on two different test patterns with pattern density variation were calculated when the patterns are pressed onto a stacked flat pad. Result showed that the pressure distribution can be well approximated with the pattern dependant oxide model. Pressure distribution from FEM was compared with the inverse of local effective pattern density, which was evaluated with different weighting functions. Planarization length was also evaluated with the pressure distribution on each of the test structure.

TEST STRUCTURE AND FINITE ELEMENT MODEL

A two dimensional static model was used for the simulation. Pattern size was 1cm, consisted of five different sections with different pattern densities varying from 6% to 50%. To prevent ex-plane moment and tilting of the entire pattern structure, the pattern was designed to be symmetric. Figure 1 shows two different patterns used for the test. Two patterns are in same size and same pattern density variation. In pattern 1, line width remains constant (25 μm) and between-line space changed for pattern density variation. In pattern 2, between-line space remains constant (200 μm) and line width changed for pattern density variation.

Pad material properties were assumed to be linear elastic. To simulate a stacked pad, two different materials, hard and soft, were assigned to two different layers of the pad. All degrees of freedom of motion at the top surface nodes of the pad were fixed as zero throughout the simulation and all degrees of freedom of motion of the top surface nodes of the bottom layer and bottom surface nodes of the top layer were tied together. The pattern was located at the bottom and the pad was located on top of it. Hard material properties were assigned to the bottom layer, which is in touch with the pattern and soft material properties were assigned to the top layer. Pressure was given on the bottom surface of the substrate toward the pad. Each pattern line has the same height and the substrate was assumed to be rigid to prevent any deformation effect from the substrate.

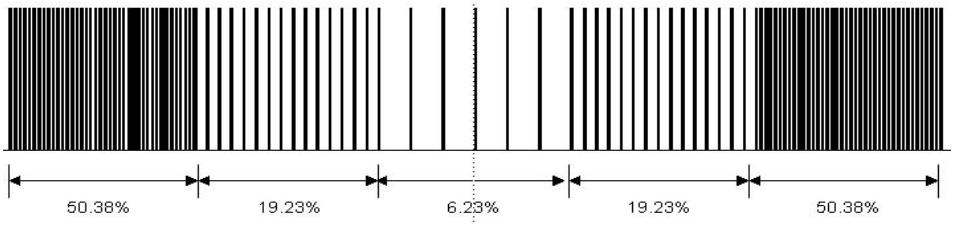

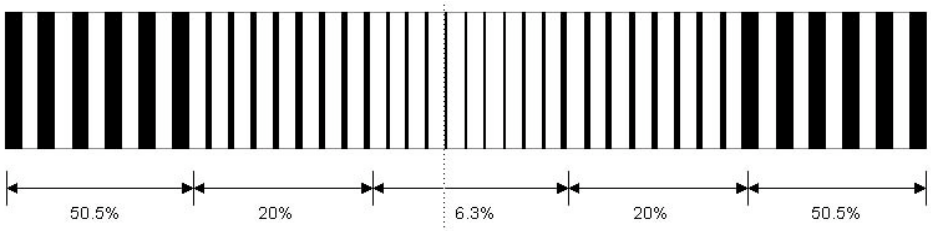

RESULT

Figure 3 shows the contact stress distribution calculated from the finite element simulation. High contact pressure is observed in the low-density region and low contact pressure is observed in the high-density region. Highest to lowest ratio in each test pattern was 5.98 for constant line width pattern and 6.87 for constant space pattern. To compare this test result with pattern density based oxide CMP model, effective local pattern density was calculated for each pattern. Figure 4 is a schematic picture that shows local pattern density evaluation at position x. Local pattern density at x is determined as the sum of the up area divided by the evaluation window area.

$$\rho(x) = \frac{\sum up\_area}{2PL} = \frac{a1+a2+a3+a4+a5+a6}{2PL} \quad (4)$$

Here, the local pattern density is dependant on the window size for local pattern density evaluation. Figure 5 show the variation of the 1/local pattern density evaluated with various window sizes. The planarization length was defined as the half of the window size.

As the window size (planarizaiton length) increases, the highest/lowest ratio of the 1/local pattern density across the pattern decreases. The half of the window size, which gives the best fit between 1/local pattern density variation and pressure distribution from FEM was defined as the planarization length of the test. The local pattern density is not only dependent upon the window size, but also dependant upon the weighting function across the window. By using a weighting function, it is possible to consider the different contributions of the pattern inside a window for a local density calculation. Three different weighting functions, step function with circular window, step function with square window, and elliptic function from pad deformation profile (Ouma et al., 2002). First, the test pattern was sectioned with 40 _m _ 40_m cells; then pattern density (PDi) was calculated for each cell. Second, convolution of the weighting function and PDi across the window was calculated for the local effective pattern density. Equation (5) and (6) shows the elliptic weighting function and effective pattern density. Figure 6 is an example of the effective pattern density map calculated over a test pattern.

$$w(r) = \frac{4(1-\gamma^2)qr}{\pi E}\int_0^{\frac{\pi}{2}}\sqrt{1-\frac{r^2}{PL^2}\sin^2\theta}\,d\theta \quad (5)$$

$$PD_E = \sum_{i,j}\left(\frac{w(i,j)\times PD(i,j)}{\sum_{i,j} w(i,j)}\right) \quad (6)$$

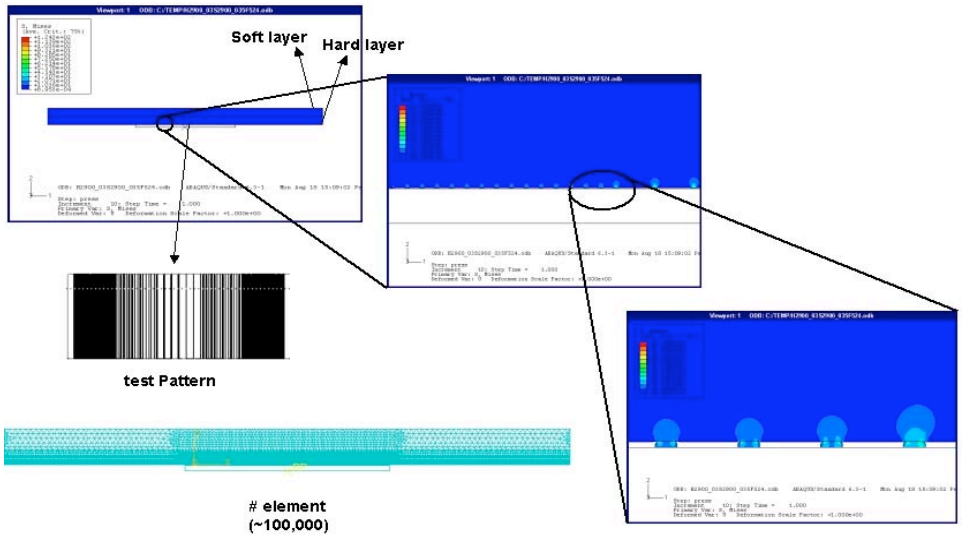

Figure 7 shows the comparison between pressure distribution from FEM and the effective pattern density with three different weighting functions for each of the test pattern, where the dotted line shows the FEM result and the solid line shows the 1/effective pattern density. Square sum error between FEM result and effective pattern density was calculated with equation (7).

Square sum error =

$$\frac{\sum_{n=1}^{K}\left\{\frac{b}{a}\frac{1}{density(n)}-P(n)\right\}^2}{n} \qquad (7)$$

The value of b/a corresponds to the Preston coefficient. The square sum error for the constant line width pattern (1.41~1.80) was much smaller than that of the constant space pattern (7.43~9.47). The effect of the weighting function was not clear.

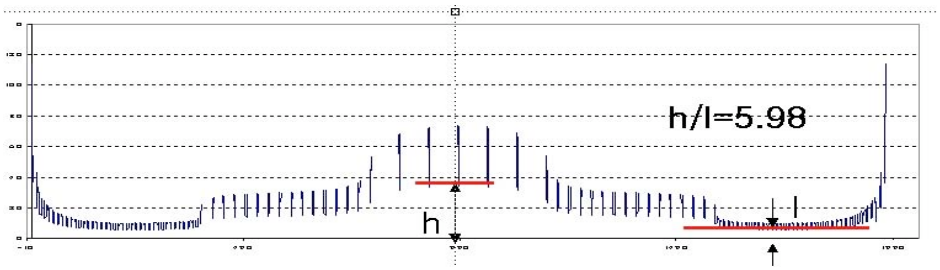

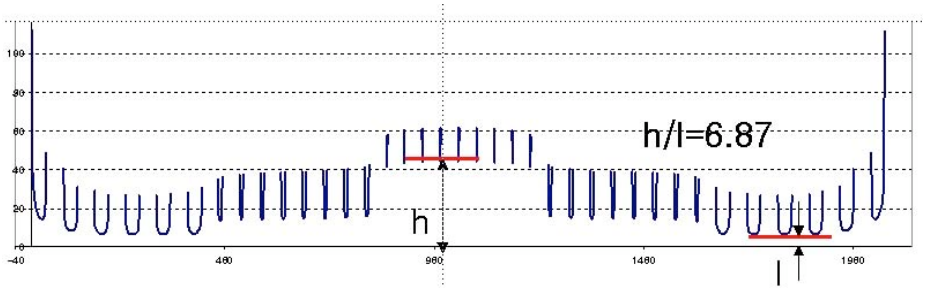

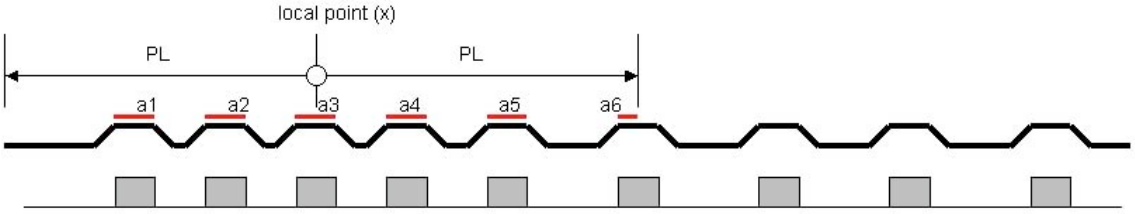

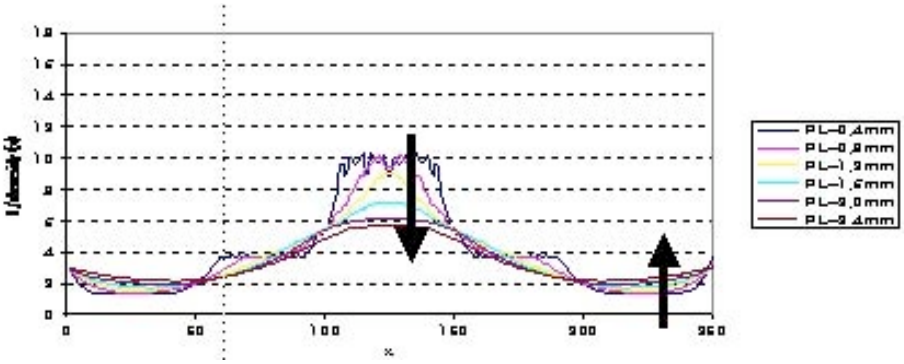

(a) Constant line width pattern

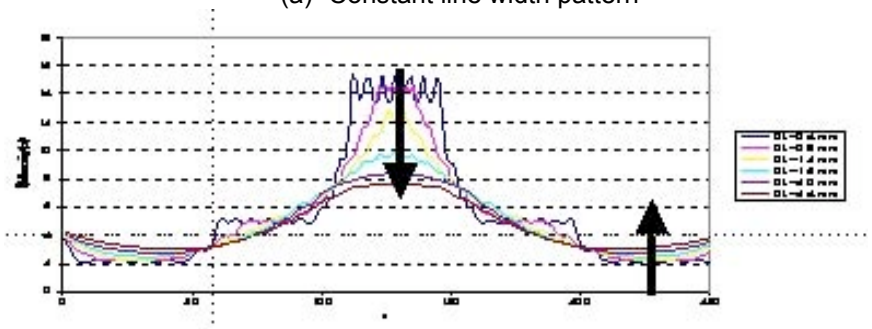

(b) Constant space pattern

FIGURE 5. 1/LOCAL PATTERN DENSITY WITH VARIOUS WINDOW SIZES. WITH LARGER WINDOW, THE VARIATION OF 1/LOCAL PATTERN DENSITY ACROSS THE PATTERN BECOMES SMOOTHER. (IE. HIGHEST/LOWEST RATIO DECREASES).

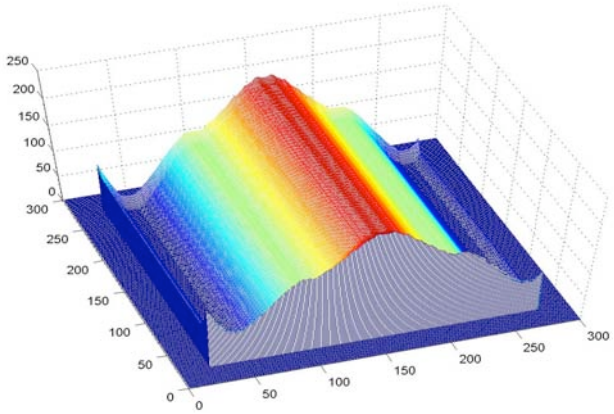

FIGURE 6. EFFECTIVE PATTERN DENSITY MAP OVER A TEST PATTERN. (Z-AXIS: 1/EFFECTIVE PATTERN DENSITY).

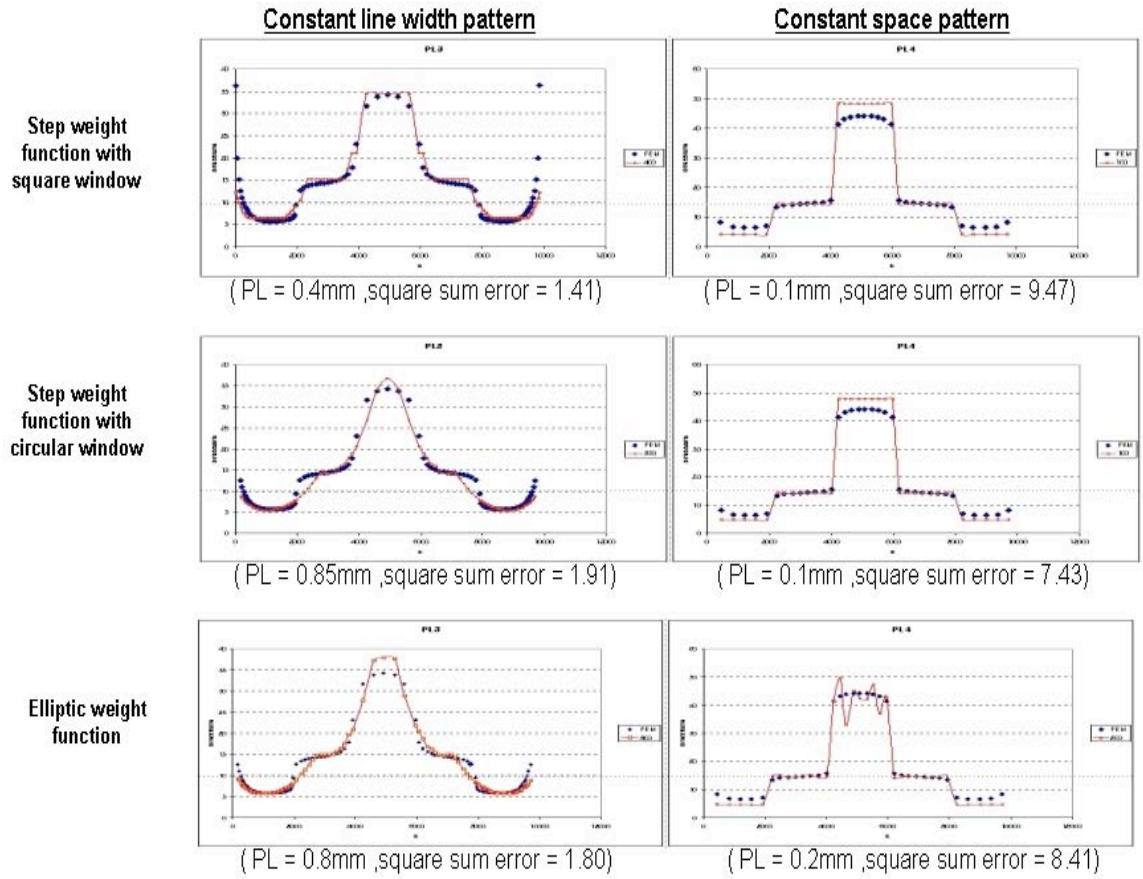

FIGURE 7. COMPARISON BETWEEN PATTERN DENSITY MODEL AND PRESSURE DISTRIBUTION FROM FEM (DOTTED LINE: FEM, SOLID LINE: PATTERN DENSITY MODEL).

REFERENCES

D. Ouma, B. Stine, R. Divecha, D. Boning, J. Chung, G. Shinn, I. Ali, and J. Clark, (1997), ``Wafer-Scale Modeling of Pattern Efect in Oxide Chemical Mechanical Polishing,'' Manufacturing Yield, Reliability, and Failure Analysis session, *SPIE 1997 Symposium on Microelectronic Manufacturing,* Austin TX, Oct.

B. Stine, D. Ouma, R. Divecha, D. Boning, J. Chung (1998), ''Rapid Characterization and Modeling of Pattern Dependent Variation in Chemical Mechanical Polishing,'' *IEEE Trans. Semi. Manuf.,* vol. 11, no. 1, pp. 129-140, Feb.

D. O. Ouma, D. S. Boning, J. E. Chung, W. G. Easter, V. Saxena, S. Misra, and A. Crevasse (2002), ``Characterization and Modeling of Oxide Chemical Mechanical Polishing Using Planarization Length and Pattern Density Concepts,'' *IEEE Transactions on Semiconductor Manufacturing*, vol. 15, no. 2, pp. 232-244, May.

Preston, F. W. (1927), "The theory and design of plate glass polishing machines," J. Soc. Glass Tech., vol. 11, pp. 214-256.